Chinese Chemical Letters 33 (2022) 229–233

Contents lists available at ScienceDirect

Chinese Chemical Letters

journal homepage: www.elsevier.com/locate/cclet

A novel conformationally adaptive macrocyclic tetramaleimide with flipping pyrene sidewalls

Lingyun Zhu[a], Wei Zeng[a], Menghua Li[a], Meijin Lin[a,b,*]

[a] Key Laboratory of Molecule Synthesis and Function Discovery, and Fujian Provincial Key Laboratory of Electrochemical Energy Storage Materials, College of Chemistry, Fuzhou University, Fuzhou 350116 China
[b] College of Materials Science and Engineering, Fuzhou University, Fuzhou 350116, China

ARTICLE INFO

Article history:
Received 10 April 2021
Revised 31 May 2021
Accepted 3 June 2021
Available online 10 June 2021

Keywords:
AEE
Conjugated macrocycles
DFT
Flipping sidewalls
Vapochromic

ABSTRACT

The synthesis, structure, and properties of pyrene-based conformationally adaptive macrocycles are described. This new type of conformationally adaptive macrocycle was constructed through Perkin reaction, followed by imidization. By changing the condensation partner as the linking unit, a family of conjugated macrocycles with different sizes of the cavity was synthesized, which provide a simple and modular synthetic strategy towards the conformationally adaptive macrocycles. Furthermore, the macrocycles provide two well-defined conformations through flipping pyrene subunit, which were unambiguously determined by single-crystal X-ray diffraction analysis. The conformational interconversion barrier was determined by density functional theory (DFT) calculations. This new macrocycle also demonstrated unique properties, such as vapochromic behavior and aggregation emission enhancement effect. Furthermore, we have also investigated the effect of the linker on the shape and photophysical properties of the resulting macrocyclic products.

Conformationally adaptive macrocycles are adaptive to guests or environmental changes, such as temperature and solvent, which have the conformational ensemble features of bioreceptors [1,2]. It has been demonstrated that the conformationally adaptive macrocycles have wide potential applications in chirality sensing [1], selected recognition [3], stimuli-responsive self-assembly [4–6], and molecular switches [7]. The development of conformationally adaptive macrocyclic has received extensive attention in recent years. There are three types of conformationally adaptive macrocycles with flipping aromatic sidewalls (Fig. 1A) [8]. For model C, the linking positions of aromatic sidewalls are the two centrosymmetric positions, and flipping one aromatic sidewall of I gives rise to a pair of enantiomers (Fig. 1B). The structural flexibility is dramatically affected by the linkers that connect the aromatic sidewalls. Hence, the representative macrocycles of model C can be divided based on linkers include aromatic linkers [9,10], CH_2–O-CH_2 linkers [11–13], CH_2 linkers [14–16] and direct linkage (Fig. 1C) [17,18]. These successful examples have encouraged us to develop a new type of conformationally adaptive macrocycles to introduce new properties to the resulting macrocycles (Fig. 1D).

Pyrene is a widely used fluorescent chromophore that possesses unique photophysical properties, for example, high fluorescence quantum yield, the tendency for excimer formation, and long fluorescence lifetime [19–23]. Hence, pyrene was selected as the aromatic sidewall in our study. Inspired by Durola's synthesis of macrocyclic conjugated oligomers [24–26], we employ pyrene as an aromatic sidewall and aryl maleimide as a linker for the synthesis of a new type of conformationally adaptive macrocycles by Perkin reaction and imidization reaction. This new macrocycle shows vapochromic behavior and aggregation emission enhancement (AEE) effect. We have also investigated the effect of the linker on the shape and photophysical properties of the resulting macrocyclic products. Finally, the conformational interconversion barrier was determined by DFT calculations as well.

The conjugated macrocycle (**MC**, Scheme 1) was synthesized by the reaction of pyrenylene-1,6-diglyoxylic acid with 1.4-phenylenediacetic acid, followed by treatment with 2,6-diisopropylaniline in 46% isolated yield over two steps as a red solid (**MC1.1**). Furthermore, to prove the generality of our synthetic approach and the diversity of accessible structures, biphenyl as a subunit of the linker was tested, which provided the corresponding macrocycles **MC2.1** in 7.9% yield, the lower yield is due to the more difficult macrocyclization caused by the rotation of the biphenyl. In addition to varying the linker, we have also tested

* Corresponding author.
E-mail address: meijin_lin@fzu.edu.cn (M. Lin).

https://doi.org/10.1016/j.cclet.2021.06.003
1001-8417/

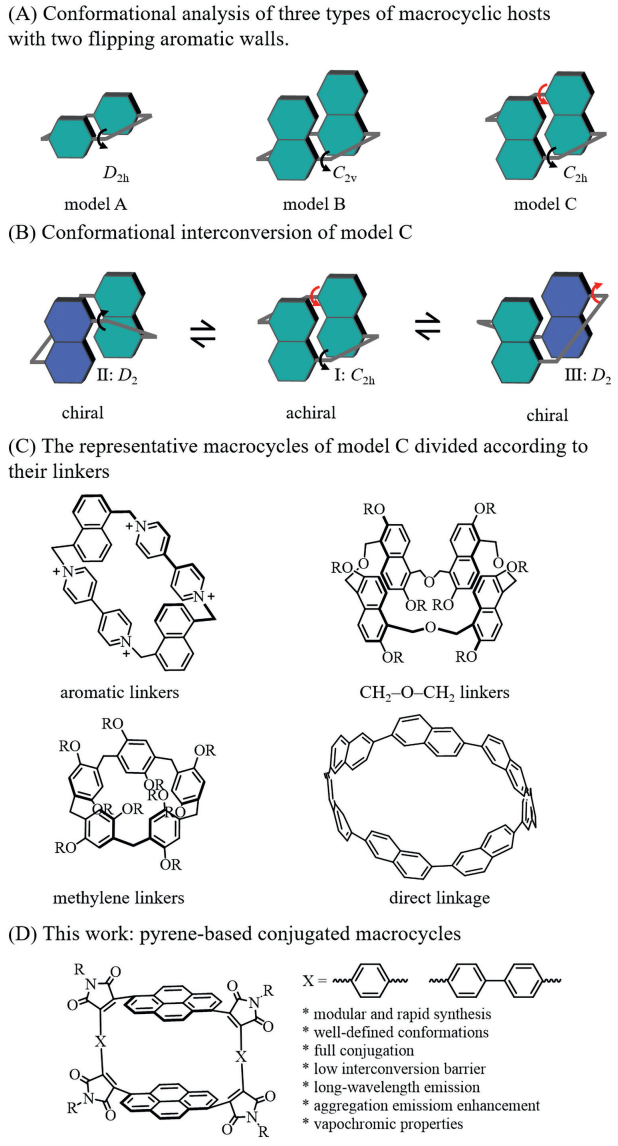

Fig. 1. Conformational analysis of three types of conformationally adaptive macrocycles.

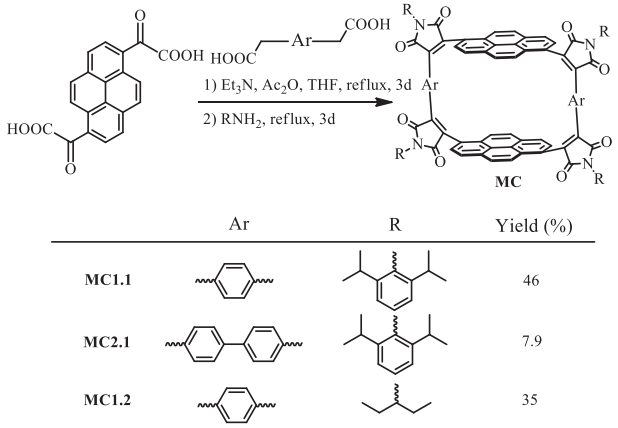

Scheme 1. Synthesis of macrocycles (**MC**).

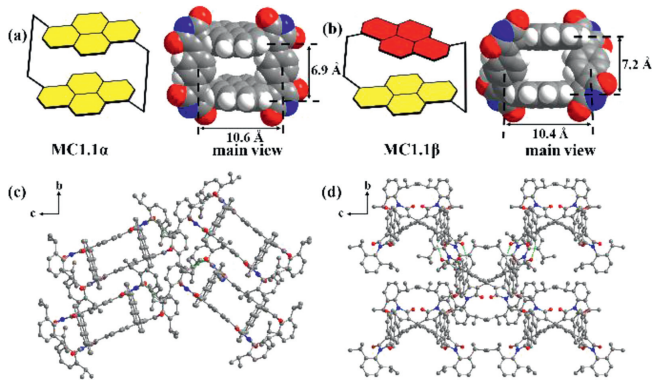

Fig. 2. (a, b) The model and main view in the space-filling model of **MC1.1*α*** and **MC1.1*β***, respectively. R group, and solvent molecules are omitted for clarity. (c, d) The packing diagram of **MC1.1*α*, MC1.1*β*** viewed along the a-axis, respectively; the green dash bonds were shortest hydrogen bonding. Unrelated hydrogen atoms and solvent molecules are omitted for clarity.

different amines, such as 1-ethylpropylamine, which provided the target product **MC1.2** in 35% yield. For comparison, acyclic fragment (**AF**) was synthesized in similar method by pyrenylene-1-glyoxylic acid and phenylacetic acid in 91% yield (Supporting information).

The conformationally adaptive macrocycle **MC1.1** with two pyrene sidewalls has three conformations: one achiral conformation (**MC1.1*α***) and a pair of planar-chiral ones (**MC1.1*β***) (Fig. 2), which are unambiguously determined by single-crystal X-ray diffraction analysis. These two different single crystals of **MC1.1** were obtained from different crystal growth methods. The yellow single crystal (**MC1.1*α***) was obtained through a solvothermal method, which dissolved with the mixture solvent in CH_3CN and CH_3OH (v:v = 1:3) and then heated at 80 °C for one day. The red single crystal (**MC1.1*β***) was obtained by its slow evaporation in the mixed solution of $CHCl_3$ and EtOH, and the same crystal form could be obtained from other mixed solutions, such as a mixed solution of ethyl acetate and *n*-pentane or a mixed solution of tetrahydrofuran and *n*-pentane.

In **MC1.1*α***, the macrocycle has two parallel and overlapping pyrene sidewalls, the distance of two pyrene's planes is 6.9 Å. Furthermore, two 1,4-phenylene sidewalls are parallel and overlapping as well, and the distance between the centers of the benzene is 10.6 Å, the angle between two different molecular layers is 45.8° The strongest noncovalent interactions are hydrogen bonding (2.724(1) Å) between the carbonyl group on the maleimide and the isopropyl group on the adjacent molecule. Compared to **MC1.1*α***, two pyrene units of **MC1.1*β*** are parallel but not overlapping, the torsion angle between the two pyrene units is 32.0°, the distance of the two planes increases to 7.2 Å. The two benzene units are intersectant, the distance between the centers of the benzene is 10.4 Å, and the dihedral angle between the two planes is 60.0° The dihedral angle between two different molecular layers is 0.9°, which is near parallel. The strongest noncovalent interactions are hydrogen bonding (2.466(7) Å) between the carbonyl group on the maleimide and the hydrogen on the intramolecular pyrene, which means the **MC1.1*β*** is more stable conformation. The parallel stacking of layers in **MC1.1*β*** results in a more red-shifted color than the interlaced stacking of layers in **MC1.1*α***, explaining the difference in color between two conformations. Unfortunately, the single crystal of **MC2.1** has not been obtained after many attempts due to poor solubility.

The interconversion between achiral conformation (**MC1.1*α***) and chiral ones (**MC1.1*β***) was further studied by DFT calculation at the B3LYP/6–31G(d) level (Fig. 3). The chiral **MC1.1*β*** is thermo-

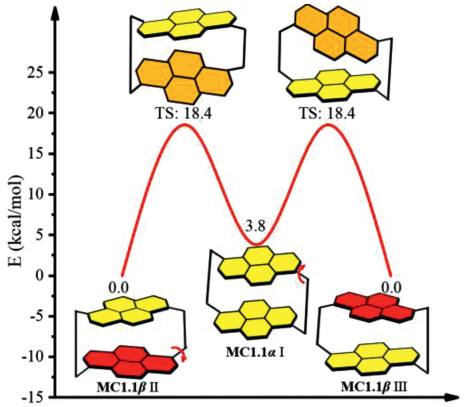

Fig. 3. The interconversion process between **MC1.1*α*** and **MC1.1*β*** and related thermal free energies was performed at the B3LYP/6–31G(d) level. The different side of the pyrene is marked with red and yellow (R is replaced by -CH_3 to simplify the calculation).

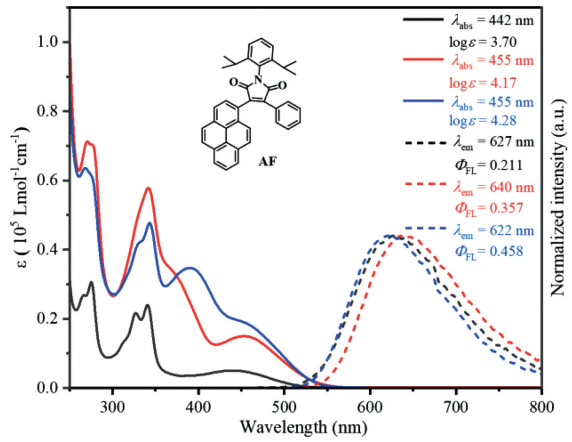

Fig. 4. UV–vis absorption (solid) and fluorescence spectra (short dash) of **AF** (black), **MC1.1** (red), **MC2.1** (blue) in dichloromethane. Concentration: 1×10^{-5} mol/L. Excitation wavelength: 450 nm for **AF** and **MC1.1**; 400 nm for **MC 2.1**.

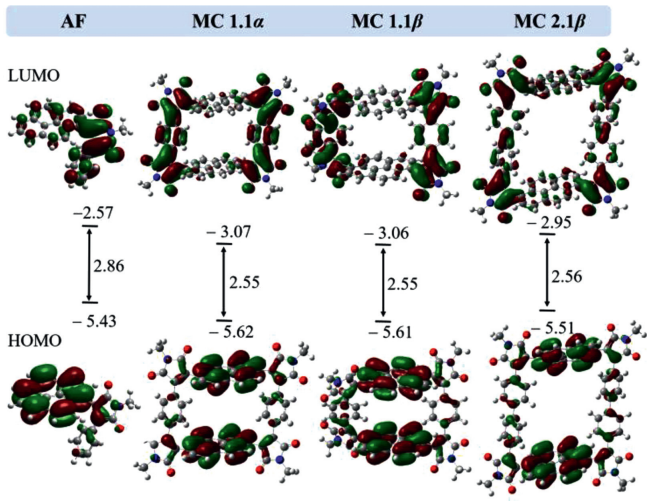

Fig. 5. The frontier orbitals of **AF, MC1.1*α*, MC1.1*β*** and **MC2.1*β***, and corresponding energy levels and energy gap calculated in Gaussian 09 at the B3LYP/6–31G(d) level by DFT. The structures of **AF, MC1.1*α*, MC1.1*β*** are optimized from the initial X-ray geometries and **MC2.1** is optimized from comformational searching. unit: eV.

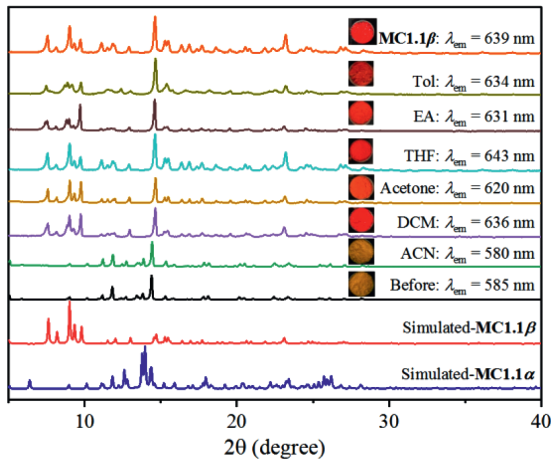

Fig. 6. The powder X-ray diffraction (PXRD) and the photographs of **MC1.1*α*** before and after adsorption different solvents. The emission wavelength of solid is marked inside. Excitation wavelength: 450 nm.

dynamically stable than achiral **MC1.1*α*** by 3.8 kcal/mol in terms of thermal free energies. For the interconversion process among these three conformations, the DFT calculation result provided a stepwise process where **MC1.1*β*II** converts into the less stable **MC1.1*α*** as the intermediate through a transition state (TS), in which the two pyrene sidewalls have the dihedral angle of 66.8°. This process subsequently was repeated on the other pyrene sidewall to give the other enantiomer **MC1.1*β*III**. The racemization barrier was estimated to be 18.4 kcal/mol at 298 K and 1 atm. Therefore, they can undergo very fast conformational interconversion at room temperature. This relatively low barrier is consistent with the result of variable temperature (VT) ^{1}H NMR, in which the diastereomeric ratio cannot be determined (Fig. S14 in Supporting information) [27].

The photophysical properties of representative macrocycles were measured (Fig. 4). Compared to acyclic fragment compound **AF** as a reference compound (λ_{em} = 627 nm), the emission spectrum of **MC1.1** (λ_{em} = 640 nm) and **MC2.1** (λ_{em} = 622 nm) were observed to have a similar emission wavelength. But the fluorescence quantum yield (Φ_{FL}) of **MC** is higher than **AF**. Due to the larger conjugate system, the absorption spectrum (λ_{abs} = 455 nm) of **MC1.1** is similar to **AF** (λ_{abs} = 442 nm) in 455 nm with triple intensity. Compared with macrocycle with non-aromatic linkers, such as crown ethers, cyclodextrins, calixarenes, and pillararenes, the conjugated macrocycles **MC** with visible light absorption and fluorescence, in which the conformational transformation with color changes makes it more practical for future application.

In order to better understand the geometric and electronic structures of **AF**, **MC1.1** and **MC2.1** on their optical properties, the quantum chemical calculations were performed by DFT calculations at the B3LYP/6–31G(d) level. The energy levels of the frontier molecular orbitals of **AF, MC1.1*α*, MC1.1*β***, and **MC2.1*β*** are shown in Fig. 5. The HOMO (highest occupied molecular orbital) and LUMO (lowest unoccupied molecular orbital) of these four compounds are separated. The HOMO of these four compounds mainly are delocalized over the pyrene subunits, and the LUMO of these four compounds are delocalized over maleimide and benzene units, which show the clear electron donor-acceptor structure. Compared with **AF**, the cyclic compounds show a lower energy of HOMO and LUMO, which means the cyclic structure could reduce the energy of LUMO to increase the reactivity [28]. Meantime the E_{gap} (E_{gap} = E_{LUMO} - E_{HOMO}) of **MC1.1** also decreases to 2.55 eV compared to 2.86 eV of **AF**.

Exposed the yellow crystallite (**MC1.1*α***) to the saturated vapor of volatile solvents, such as acetonitrile (ACN), dichloromethane (DCM), acetone, ethyl acetate (EA), tetrahydrofuran (THF), toluene

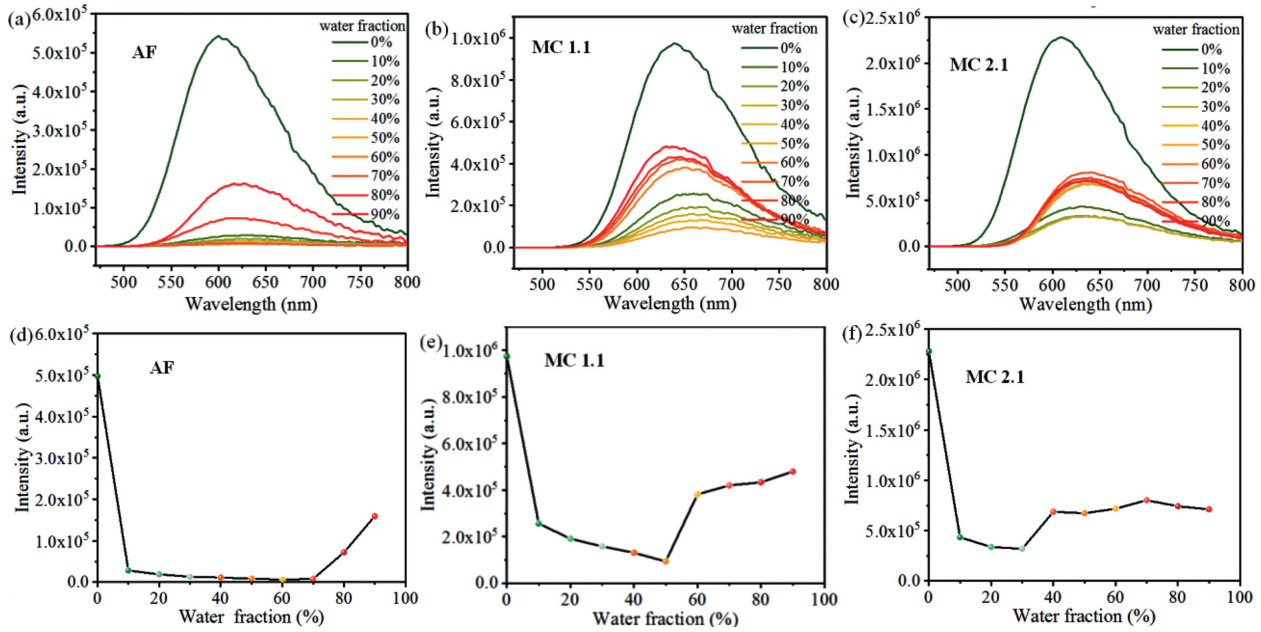

Fig. 7. (a-c) The fluorescence spectra of **AF, MC1.1, MC2.1** in different water fraction of mixed solvent of water-THF, respectively. (d-f) The max emission intensity of **AF, MC1.1, MC2.1** in different water fraction of mixed solvent of water-THF, respectively ($c = 1 \times 10^{-5}$ mol/L, excitation wavelength: 450 nm for **AF** and **MC1.1**; 400 nm for **MC2.1**).

(Tol) for overnight, the color of crystallite changed from yellow to red except the crystallite in the saturated vapor of ACN (Fig. 5). The reason for the color of crystallite did not change in ACN vapor might be that **MC1.1α** is insoluble in ACN. Checked with powder X-ray diffraction (PXRD), the crystal form has changed from α to β in red crystallite (Fig. 6). The emission wavelength has also red-shifted from 585 nm to ~640 nm in red crystallite (Fig. 6 and Fig. S19 in Supporting information). It means that the color changes only when the crystal form transforms. However, the more stable β crystal could not transform to α after many attempts, which is consistent with the DFT calculation result. The vapor of solvent could induce flipping of pyrene sidewall to give another conformation along with color change, which suggests that **MC** would be a prominent material for environmental management and industrial production monitoring.

Considering that **MC1.1** has the behavior of flipping aromatic sidewalls in the solid state, we wonder if different solvent can affect the spectra behavior of **MC1.1** and **AF**. As shown in Fig. S16 (Supporting information), both of **MC1.1** and **AF** exhibit quite similar absorption maxima and spectral shapes in different solvent. However, the tremendous differences in different solvent appeared in their emission spectra, the emission maximum red-shifted and the fluorescent intensity decreased with the fluorescence quantum yields decreased (Table S2 in Supporting information) when increase the solvent polarity, which indicated that **MC1.1** and **AF** underwent a typical twisted intramolecular charge transfer (TICT) process in polar solvent. To better understand the existence of TICT process in different solvents, the dependence of the Stokes shifts ($\Delta\upsilon$) *vs.* the solvent polarity paramater (Δf) was investigated, the linear relationship between $\Delta\upsilon$ and Δf in higher polar solvent suggesting that the TICT process of **MC1.1** and **AF** could be achieved in polar solvent (Fig. S17 in Supporting information).

Besides TICT effects, it seems that **MC**s and **AF** also exhibit aggregation-induced emission (AIE) or AEE features in poor solvent. Indeed, the fluorescence spectra of the three compounds in the THF (good solvent) and water (poor solvent) mixed solvents with different water fractions were investigated. As shown in Fig. 7, **AF** exhibits AIE feature, and **MC**s exhibit AEE features. As for **AF**, the fluorescence intensity was gradually quenched with the increase of water fraction in the mixed solvent to 70%, and then the fluorescence intensity was gradually enhanced with the further increase of water fraction. And in the case of **MC1.1** and **MC1.2**, with the increase of the ratio of water in the mixed solvent, the fluorescence intensity first gradually decreased and then gradually increased. This is because there is a competition between TICT and AEE effects. When water fraction is low, there is no aggregation in the mixture solvent and TICT effect is dominant which induced the fluorescence intensity quenched and emission red-shifted [29,30]. However, when water fraction was further increased, the formation of aggregates suppressed the TICT process and enhanced the AEE effect, as the result, the fluorescence intensity enhanced and emission blue-shifted.

In summary, we have developed an efficient synthetic strategy to synthesize a novel conformationally adaptive macrocycle linked with four maleimide units at the corners, which has two well-defined conformations (chiral and achiral one). The interconversion barriers of these conformations were estimated by DFT calculations. The particular advantages of this new conformationally adaptive macrocycles are their long-wavelength emission, AEE emission, and vapochromic behavior. In a broader perspective, different conjugated macrocycles skeleton will be synthesized and modified with various functional group in maleimides, which will have potential application in host-guest chemistry, circularly polarized luminescence (CPL) dyes and bioimage. Further exploration in this direction is ongoing in our group.

Declaration of competing interest

The authors declare that they have no known competing financial interests or personal relationships that could have appeared to influence the work reported in this paper.

Acknowledgments

This work is supported by the National Natural Science Foundation of China (Nos. 21971041 and 22001039), Natural Science Foundation of Fujian Province (Nos. 2018J01431, 2018J01690 and

2020J01447), and Research Foundation of Education Bureau of Fujian Province (No. JT180813).

Supplementary materials

Supplementary material associated with this article can be found, in the online version, at doi:10.1016/j.cclet.2021.06.003.

References

[1] L.L. Wang, M. Quan, T.L. Yang, Z. Chen, W. Jiang, Angew. Chem. Int. Ed. 59 (2020) 23817–23824.
[2] Q. Li, H. Zhu, F. Huang, J. Am. Chem. Soc. 141 (2019) 13290–13294.
[3] L.L. Wang, Y.K. Tu, A. Valkonen, K. Rissanen, W. Jiang, Chin. J. Chem. 37 (2019) 892–896.
[4] X. Yao, J. Mu, L. Zeng, et al., Mater. Horiz. 6 (2019) 846–870.
[5] A. Blanco-Gomez, P. Corton, L. Barravecchia, et al., Chem. Soc. Rev. 49 (2020) 3834–3862.
[6] L.P. Yang, L. Zhang, M. Quan, et al., Nat. Commun. 11 (2020) 2740.
[7] T. Ogoshi, R. Shiga, T.A. Yamagishi, Y. Nakamoto, J. Org. Chem. 76 (2011) 618–622.
[8] X. Wang, F. Jia, L.P. Yang, H. Zhou, W. Jiang, Chem. Soc. Rev. 49 (2020) 4176–4188.
[9] B. Odell, M.V. Reddington, A.M.Z. Slawin, et al., Angew. Chem. Int. Ed. 27 (1988) 1547–1550.
[10] Q.H. Guo, J. Zhou, H. Mao, et al., J. Am. Chem. Soc. 142 (2020) 5419–5428.
[11] F. Jia, Z. He, L.P. Yang, et al., Chem. Sci. 6 (2015) 6731–6738.
[12] F. Jia, H.Y. Wang, D.H. Li, L.P. Yang, W. Jiang, Chem. Commun. 52 (2016) 5666–5669.
[13] F. Jia, H. Hupatz, L.P. Yang, et al., J. Am. Chem. Soc. 141 (2019) 4468–4473.
[14] K. Jie, M. Liu, Y. Zhou, et al., J. Am. Chem. Soc. 140 (2018) 6921–6930.
[15] J. Ji, Y. Li, C. Xiao, et al., Chem. Commun. 56 (2020) 161–164.
[16] X. Zhang, X. Wang, B. Wang, Z.J. Ding, C. Li, Chin. Chem. Lett. 31 (2020) 3230–3232.
[17] Z. Sun, P. Sarkar, T. Suenaga, S. Sato, H. Isobe, Angew. Chem. Int. Ed. 54 (2015) 12800–12804.
[18] A. Yagi, Y. Segawa, K. Itami, J. Am. Chem. Soc. 134 (2012) 2962–2965.
[19] S. Reiter, M.K. Roos, R. Vivie Riedle, ChemPhotoChem 3 (2019) 881–888.
[20] A. Yagi, G. Venkataramana, Y. Segawa, K. Itami, Chem. Commun. 50 (2014) 957–959.
[21] X. Feng, Z. Xu, Z. Hu, et al., J. Mater. Chem. C 7 (2019) 2283–2290.
[22] Q. Lu, G.K. Kole, A. Friedrich, et al., J. Org. Chem. 85 (2020) 4256–4266.
[23] X. Chang, Z. Zhou, C. Shang, et al., J. Am. Chem. Soc. 141 (2019) 1757–1765.
[24] P. Sarkar, F. Durola, H. Bock, Chem. Commun. 49 (2013) 7552–7554.
[25] A. Robert, P. Dechambenoit, H. Bock, F. Durola, Can. J. Chem. 95 (2017) 450–453.
[26] G. Naulet, A. Robert, P. Dechambenoit, H. Bock, F. Durola, Eur. J. Org. Chem. (2018) 619–626.
[27] Y. Li, A. Yagi, K. Itami, J. Am. Chem. Soc. 142 (2020) 3246–3253.
[28] C. Liu, G. Yang, Y. Si, Y. Liu, X. Pan, J. Mater. Chem. C 5 (2017) 3495–3502.
[29] S. Sasaki, S. Suzuki, K. Igawa, K. Morokuma, G.I. Konishi, J. Org. Chem. 82 (2017) 6865–6873.
[30] J. Li, J. Wang, H. Li, et al., Chem. Soc. Rev. 49 (2020) 1144–1172.